# Bright solitons in a two-dimensional spin-orbit-coupled dipolar Bose-Einstein condensate

Yong Xu,[1] Yongping Zhang,[2] and Chuanwei Zhang[1,*]
[1]*Department of Physics, The University of Texas at Dallas, Richardson, Texas 75080, USA*
[2]*Quantum Systems Unit, OIST Graduate University, Onna, Okinawa 904-0495, Japan*
(Received 8 May 2015; published 27 July 2015)

We study a two-dimensional spin-orbit-coupled dipolar Bose-Einstein condensate with repulsive contact interactions by both the variational method and the imaginary-time evolution of the Gross-Pitaevskii equation. The dipoles are completely polarized along one direction in the two-dimensional plane to provide an effective attractive dipole-dipole interaction. We find two types of solitons as the ground states arising from such attractive dipole-dipole interactions: a plane-wave soliton with a spatially varying phase and a stripe soliton with a spatially oscillating density for each component. Both types of solitons possess smaller size and higher anisotropy than the soliton without spin-orbit coupling. Finally, we discuss the properties of moving solitons, which are nontrivial because of the violation of Galilean invariance.

DOI: 10.1103/PhysRevA.92.013633 PACS number(s): 03.75.Lm, 03.75.Mn, 71.70.Ej

## I. INTRODUCTION

Ever since the first achievement of Bose-Einstein condensates (BECs) in ultracold atomic gases [1–3], matter wave solitons in these systems have been the central focus of many experiments and theory [4]. Solitons that keep their shape while traveling are the result of the interplay between nonlinearity and dispersion. In BECs, nonlinearity usually originates from short-range collisional interactions between atoms, which can be readily tuned via Feshbach resonances [5]. In general, there are two types of solitons: a bright soliton with a density bump and a dark soliton with a density notch as well as a phase jump [4]. For pure contact interactions, a bright and a dark soliton can emerge, respectively, when the interactions are attractive or repulsive. Both these solitons have been experimentally observed in cold atoms [6–14]. However, for these contact attractive interactions, bright solitons can only exist in one dimension, but not in two dimensions, where the states either collapse or expand [15].

Different from the local nonlinearity resulting from contact interactions, the nonlocal nonlinearity, in particular, the nonlinearity introduced by the dipole-dipole interaction, can stabilize a two-dimensional (2D) bright soliton [16,17]. The dipole interaction is long range and anisotropic with the strength and sign (i.e., repulsive or attractive) depending on the dipole orientation. When an external rotating magnetic field is applied to reverse the sign of the interaction [18] or the dipoles are completely polarized in a 2D plane [19], the dipolar interaction can become attractive and 2D bright solitons can therefore be stabilized under appropriate conditions (i.e., the ground state of the system is a bright soliton with a localized density profile). It is essential to note that although the relevant interaction in most experiments with cold atomic gases is contact, increasing interest has been focused on the atoms with large magnetic moments that possess dipole-dipole interactions [17,20,21]. In fact, the Bose-Einstein condensation of several dipolar atoms such as chromium [22–24], dysprosium [25], and erbium [26] and the degeneracy of a dipolar Fermi gas [27,28] have been observed in experiments.

Recently, the spin-orbit coupling between two hyperfine states of cold atoms has been experimentally engineered [29–34]. This achievement has ignited tremendous interest in this field because of the dramatic change in the single-particle dispersion (induced by spin-orbit coupling), which in conjunction with the interaction leads to many exotic superfluids [35–46] (also see [47–54] for reviews). Such change in dispersion also results in exotic solitons even when the interaction is contact (without dipole-dipole interactions), including 1D bright solitons [55–61] for a BEC with attractive contact interactions, 1D dark [62,63] and gap solitons [64–66] for a BEC with repulsive contact interactions, and 1D dark solitons for Fermi superfluids [67,68]. These solitons exhibit unique features that are absent without spin-orbit coupling, for instance, the plane-wave profile with a spatially varying phase and the stripe profile with a spatially oscillating density for BECs, as well as the presence of Majorana fermions inside a soliton for Fermi superfluids. Also, the violation of Galilean invariance [56,69,70] by spin-orbit coupling dictates that the structure of solitons changes with their velocities.

On the other hand, spin-orbit-coupled BECs with dipole-dipole interactions [71–74] have also been explored and intriguing quasicrystals [75] as well as meron states [76] have been found (these ground states are extended and not localized bright solitons). However, whether a soliton can exist in such BECs in two dimensions with both long-range dipole-dipole interactions and spin-orbit dispersion has not yet been investigated.

In this paper we examine the existence and properties of a bright soliton in a two-species spin-orbit-coupled dipolar BEC in two dimensions with repulsive contact interactions via both the variational method and the imaginary-time evolution of the Gross-Pitaevskii equation (GPE). The dipoles are completely oriented along the $y$ direction in the 2D plane [i.e., the $(x,y)$ plane] in order to provide an effective attractive dipole-dipole interaction. Due to such attractive interactions, we find two types of solitons: a plane-wave soliton (when the repulsive intraspecies contact interaction is larger than the repulsive interspecies one) and a stripe soliton (when the interspecies one is larger). These 2D solitons are the ground states of the system and they cannot exist as the ground states of a system with purely attractive contact interactions (no dipole)

*chuanwei.zhang@utdallas.edu

 

and spin-orbit coupling. Such solitons are highly anisotropic and their size is also reduced by spin-orbit coupling. Finally, we study the moving solitons, which are nontrivial because of the lack of Galilean invariance. The size of a soliton first increases and then decreases with the rise of the velocity and this change is anisotropic. The moving soliton also tends to be plane wave even when its stationary counterpart has the stripe structure.

The paper is organized as follows. In Sec. II we introduce the energy functional and the time-dependent GPE, which are used to describe a spin-orbit-coupled dipolar BEC. In Sec. III we calculate the ground states that are bright solitons by performing the minimization of the energy of the variational ansatz wave functions and an imaginary-time evolution of the GPE. The properties of such soliton are also explored by the former method. Then we study the nontrivial moving solitons in Sec. IV. Finally, we summarize in Sec. V.

## II. MODEL

We consider a Rashba-type spin-orbit-coupled BEC [47,51] and write its single-particle Hamiltonian as

$$H_s = \frac{\hat{\mathbf{p}}^2}{2m} + \frac{1}{2}m\omega_\perp^2\rho^2 + \frac{1}{2}m\omega_z^2 z^2 + \lambda(\hat{\mathbf{p}}\times\boldsymbol{\sigma})\cdot\mathbf{e}_z, \quad (1)$$

where $\rho = \sqrt{x^2+y^2}$, $\hat{\mathbf{p}} = -i\hbar\nabla$ is the momentum operator, $m$ is the atom mass, $\lambda$ is the spin-orbit coupling strength, $\boldsymbol{\sigma}$ are Pauli matrices, $\mathbf{e}_z$ is a unit vector along the $z$ direction, and $\omega_\perp$ ($\omega_z$) is the trap frequency in the $(x,y)$ plane (along the $z$ direction). Here we assume that $\hbar\omega_z$ is much larger than $\hbar\omega_\perp$ and the mean-field interaction so that the atoms are frozen to the ground state in the $z$ direction. Given that a soliton is studied, we thus set $\omega_\perp = 0$.

When the $s$-wave contact and dipole-dipole interactions are involved, the energy functional of a 2D condensate can be written as

$$E = \int d\mathbf{r}\Big[\Psi(\mathbf{r})^\dagger H_s\Psi(\mathbf{r}) + \frac{1}{2}g(|\Psi_\uparrow|^4 + |\Psi_\downarrow|^4) + g_{12}|\Psi_\uparrow|^2|\Psi_\downarrow|^2\Big] + E_{dd}, \quad (2)$$

where the condensate wave function $\Psi(\mathbf{r}) = [\Psi_\uparrow(\mathbf{r}),\Psi_\downarrow(\mathbf{r})]^T$ with two pseudospin components $\Psi_{\uparrow(\downarrow)}(\mathbf{r})$ and $g = 4\pi\hbar^2 a/\sqrt{2\pi}l_z m$ and $g_{12} = 4\pi\hbar^2 a_{12}/\sqrt{2\pi}l_z m$ are the intraspecies and interspecies contact interaction strengths, respectively, with the intraspecies and interspecies $s$-wave scattering length being $a$ and $a_{12}$ and the characteristic length along $z$ being $l_z = \sqrt{\hbar/m\omega_z}$. Here $H_s = -\hbar^2(\partial_x^2+\partial_y^2)/2m - i\hbar\lambda(\partial_x\sigma_y - \partial_y\sigma_x)$ is the 2D single-particle Hamiltonian and the third dimension has been integrated out. For dipole-dipole interactions, we only consider the density-density interaction, which is dominant when a two-subspace (i.e., two pseudospin states) of a large spin atom (e.g., dysprosium) is considered. We also assume that the dipoles are all oriented along the $y$ direction, thus

$$E_{dd} = \frac{g_d}{2}\frac{1}{(2\pi)^2}\int d\mathbf{k}\rho_{\mathbf{k}}\rho_{-\mathbf{k}}U_d(\mathbf{k}l_z), \quad (3)$$

where the Fourier transform of the total density is $\rho_{\mathbf{k}} = \int d\mathbf{r}e^{-i\mathbf{k}\cdot\mathbf{r}}(|\Psi_\uparrow|^2 + |\Psi_\downarrow|^2)$ and $U(\mathbf{k})$ is given by [18]

$$U_d(\mathbf{k}l_z) = -\sqrt{2\pi} + \frac{3\pi l_z k_y^2 e^{k^2 l_z^2/2}\,\mathrm{erfc}(kl_z/\sqrt{2})}{k}, \quad (4)$$

with erfc being the complementary error function. Here $g_d = \mu_0\mu^2/6\pi l_z$ characterizes the strength of the dipole-dipole interaction where $\mu$ is the magnetic dipolar moment and $\mu_0$ is the permeability of the free space. We note that this head-to-tail dipole configuration that can be attractive is different from the head-to-head configuration in Ref. [75] that is repulsive.

The dynamical behavior of a BEC can be described by the time-dependent GPE

$$i\hbar\frac{\partial\Psi(\mathbf{r})}{\partial t} = H_s\Psi(\mathbf{r}) + gG\Psi(\mathbf{r}) + g_d U_d(\mathbf{r})\Psi(\mathbf{r}), \quad (5)$$

where the contact interaction matrix is

$$G = \begin{pmatrix} |\Psi_\uparrow|^2 + \frac{g_{12}}{g}|\Psi_\downarrow|^2 & 0 \\ 0 & |\Psi_\downarrow|^2 + \frac{g_{12}}{g}|\Psi_\uparrow|^2 \end{pmatrix} \quad (6)$$

and the dipolar interaction potential is

$$U_d(\mathbf{r}) = \frac{1}{(2\pi)^2}\int d\mathbf{k}e^{i\mathbf{k}\cdot\mathbf{r}}\rho(\mathbf{k})U_d(\mathbf{k}l_z). \quad (7)$$

For numerical simulation, we choose $\hbar\omega_z$, $l_z$, and $1/\omega_z$ as the units of energy, length, and time, respectively, and the dimensionless energy per atom hence reads

$$\mathcal{E} = \int d\mathbf{r}\Big[\Phi(\mathbf{r})^\dagger\mathcal{H}_s\Phi(\mathbf{r}) + \frac{1}{2}\gamma(|\Phi_\uparrow|^4 + |\Phi_\downarrow|^4) + \gamma_{12}|\Phi_\uparrow|^2|\Psi_\downarrow|^2\Big] + \frac{\gamma_d}{2(2\pi)^2}\int d\mathbf{k}n_{\mathbf{k}}n_{-\mathbf{k}}U_d(\mathbf{k}), \quad (8)$$

where $\mathcal{H}_s = -(\partial_x^2+\partial_y^2)/2 - i\alpha(\partial_x\sigma_y - \partial_y\sigma_x)$, $\alpha = \lambda/\omega_x l_z$, $\gamma = 2\sqrt{2\pi}N_0 a/l_z$, $\gamma_{12} = 2\sqrt{2\pi}N_0 a_{12}/l_z$ with the total particle number $N_0$, $\gamma_d = 2N_0 a_d/l_z$ with $a_d = m\mu_0\mu^2/12\pi\hbar^2$, and $n_{\mathbf{k}} = \int d\mathbf{r}e^{-i\mathbf{k}\cdot\mathbf{r}}(|\Phi_\uparrow|^2 + |\Phi_\downarrow|^2)$. The wave function is normalized to 1 [i.e., $\int d\mathbf{r}(|\Phi_\uparrow|^2 + |\Phi_\downarrow|^2) = 1$]. The dimensionless time-dependent GPE reads

$$i\frac{\partial\Phi(\mathbf{r})}{\partial t} = \mathcal{H}_s\Phi(\mathbf{r}) + \gamma\mathcal{G}\Phi(\mathbf{r}) + \frac{\gamma_d}{(2\pi)^2}\int d\mathbf{k}e^{i\mathbf{k}\cdot\mathbf{r}}n(\mathbf{k})U_d(\mathbf{k})\Phi(\mathbf{r}), \quad (9)$$

where

$$\mathcal{G} = \begin{pmatrix} |\Phi_\uparrow|^2 + \frac{\gamma_{12}}{\gamma}|\Phi_\downarrow|^2 & 0 \\ 0 & |\Phi_\downarrow|^2 + \frac{\gamma_{12}}{\gamma}|\Phi_\uparrow|^2 \end{pmatrix}. \quad (10)$$

## III. STATIONARY BRIGHT SOLITONS

To shed light on the structure of a soliton, we start from a Rashba spin-orbit-coupled single-particle system in the absence of interactions in a free space and write its momentum space dispersion as

$$E(\mathbf{k}) = \frac{\mathbf{k}^2}{2} \pm \alpha k, \quad (11)$$

with two branches labeled by the helicity $\pm$, which is the eigenvalue of $(k_x\sigma_y - k_y\sigma_x)/k$, where $k = \sqrt{k_x^2 + k_y^2}$. Clearly, the ground state is degenerate with the energy being $-\alpha^2/2$ when the momenta lie in the $k = |\alpha|$ ring. This is different from the case without spin-orbit coupling where the ground state only occurs at $k = 0$. In this single-particle case, any superposition of the states in the ring is also its ground state. Yet this is not the case when the repulsive contact interaction is involved. The ground state possesses either a single momentum (i.e., plane-wave phase) when $\gamma_{12}/\gamma < 1$ or two opposite momenta (i.e., stripe phase) when $\gamma_{12}/\gamma > 1$ [36]. When the dipolar interaction is turned on, one may expect two types of ground states—plane-wave and stripe solitons—due to this effective long-range attractive interaction along with contact repulsive interaction.

To examine whether the ground state can indeed be a bright soliton in the spin-orbit-coupled dipolar BECs, we first consider a plane-wave soliton variational ansatz

$$\Phi_P = \begin{pmatrix} \Phi_0(x_0/2) \\ -\Phi_0(-x_0/2) \end{pmatrix} \exp(-i\mathbf{J}_p \cdot \mathbf{r}), \tag{12}$$

where

$$\Phi_0(x_0) = \frac{(a_x a_y)^{1/4}}{\sqrt{2\pi}} e^{-[a_x(x-x_0)^2 + a_y y^2]/2}. \tag{13}$$

Here $\mathbf{r} = x\mathbf{e}_x + y\mathbf{e}_y$ with unit vectors $\mathbf{e}_x$ and $\mathbf{e}_y$ along the $x$ and $y$ directions, respectively, $\mathbf{J}_p = J_p\mathbf{e}_y$ is the wave vector of the plane-wave soliton, $l_\nu = 1/\sqrt{a_\nu}$ with $\nu = x, y$ is the size of the soliton, and $x_0$ is the separation distance between two components. When $x_0 = 0$, this state is an eigenstate of $p_y\sigma_x$ multiplied by a Gaussian profile $\Phi_0(0)$ and $J_p = \alpha$ yields the minimum energy. In fact, $x_0$ is usually nonzero because of a force acting on the BEC by spin-orbit coupling $\mathbf{F} = \alpha^2(\mathbf{p} \times \mathbf{e_z})\sigma_\mathbf{z}$ [40,77], which is opposite along the $x$ direction when $\mathbf{p}$ (here $\mathbf{J}_p$) is along the $y$ direction.

In writing down the ansatz (12), we have assumed that the wave vector of the plane-wave soliton is in the $y$ direction. The prerequisite of this assumption is that the rotation symmetry [40,41] about the $z$ axis has been broken by the dipole-dipole interaction. Indeed, without the dipole-dipole interaction, this state with $\mathbf{J}_p$ along $y$ is not special and other states with $\mathbf{J}_p$ along other directions are degenerate with it. For example, the state with $\mathbf{J}_p$ along $y$ has the same energy as a state with $\mathbf{J}_p$ along $x$. Yet, with the specific dipole-dipole interaction arising from the dipoles entirely oriented along $y$, the symmetry is broken and the ground state should be elongated along $y$ ($a_x > a_y$) so as to provide an effective attractive interaction because of the head-to-tail configuration of polarized dipoles. This elongated configuration allows the existence of a 2D soliton [19] and also requires the wave vector to be along $y$ [78].

Although the wave vector $\mathbf{J}_p$ of the ground state is along $y$, there are still two options: negative and positive directions in terms of the time-reversal symmetry $\mathcal{T}$ (i.e., $-i\sigma_y\mathcal{K}$ with the complex conjugate operator $\mathcal{K}$). Specifically, the state $\Phi_{P2} = \mathcal{T}\Phi_P$ is degenerate with $\Phi_P$. In the absence of interactions, all superposition states of $\Phi_P$ and $\Phi_{P2}$,

$$\Phi_{PS} = |\cos\theta|\Phi_P + |\sin\theta|e^{i\varphi}\Phi_{P2}, \tag{14}$$

are degenerate. This degeneracy may be broken by the interaction so that the ground state is either $\Phi_P$ or $\Phi_{P2}$ or a certain superposition state of them; however, this degeneracy breaking should not happen at $\gamma_{12}/\gamma = 1$ since the interaction energy only depends on the total density, which is independent of $\theta$ and $\varphi$. This gives us an intuitive understanding that $\gamma_{12}/\gamma = 1$ may separate the plane-wave state ($|\cos\theta| = 0$ or 1) and the stripe one ($|\cos\theta| = |\sin\theta|$), similar to the homogenous spin-orbit-coupled BEC [36] without dipole-dipole interactions. For the stripe state, we note that $\varphi = 0, \pi$ corresponds to the ground state as the energy contributed by $\varphi$ is $-\gamma_{12}\sqrt{a_x a_y}e^{-(a_x x_0^2/2 + 2J_p^2/a_y)}\cos(2\varphi)/16\pi$ [79].

To evaluate the variational parameters $a_x$, $a_y$, $x_0$, $J_p$, and $\theta$, we minimize the energy $\mathcal{E}$ after substituting $\Phi_{PS}$ from Eq. (14) in Eq. (8). Indeed, the calculated variational solutions reveal that there are two types of ground states: plane-wave states when $\gamma_{12}/\gamma < 1$ and stripe states when $\gamma_{12}/\gamma > 1$. These ground states are bright solitons with localized density profiles as shown in Fig. 1; we therefore call these ground states plane-wave solitons and stripe solitons. In Figs. 1(a1)–1(el), the density and phase profiles of a typical plane-wave soliton (we choose $\theta = \varphi = 0$) are presented and the stripe structure of the phase of both two components reveals the plane-wave feature. The soliton is highly elongated along the $y$ direction and the centers of two components are spatially separated along the $x$ direction because of nonzero $x_0$. To confirm that this variational solution can qualitatively characterize the ground state of the system, we numerically compute the ground state by an imaginary-time evolution of the GPE (9). This exact numerical solution also concludes that $\gamma_{12}/\gamma < 1$ yields the plane-wave soliton, while $\gamma_{12}/\gamma > 1$ the stripe one. In Figs. 1(a2)–1(e2), we also plot the corresponding density and phase profiles of the Gross-Pitaevskii-obtained plane-wave soliton. The variational ansatz is in qualitative agreement with it given the separated centers and the plane-wave varying phase that both states possess. Yet the shape of the soliton obtained by the imaginary-time evolution deviates slightly from the Gaussian and the size is also slightly smaller.

When $\theta = \pi/4$ and $\varphi = 0$, $\Phi_{PS}$ is a stripe soliton state with a density oscillation along the $y$ direction for each component. In addition, there is no stripe for the total density. Along the $x$ direction, two components are not spatially separated and the phase for the spin $\uparrow$ reverses suddenly across $x = 0$. Following these properties by replacing $[\Phi_0(x_0/2) + \Phi_0(-x_0/2)]/\sqrt{2}$ with $\cos(J_x x)\Phi_0(0)$ and $[\Phi_0(x_0/2) - \Phi_0(-x_0/2)]/\sqrt{2}$ with $\sin(J_x x)\Phi_0(0)$ in Eq. (14), we obtain another better variational ansatz for the stripe soliton

$$\Phi_S = \Gamma\Phi_0(0), \tag{15}$$

where

$$\Gamma = \begin{pmatrix} \cos(J_y y)\cos(J_x x) - i\sin(J_y y)\sin(J_x x) \\ \cos(J_y y)\sin(J_x x) + i\sin(J_y y)\cos(J_x x) \end{pmatrix}, \tag{16}$$

with the variational parameters $J_x$ and $J_y$. The period of the stripe along the $y$ direction is $\pi/J_y$. Interestingly, this stripe soliton corresponds to four points $(\pm J_x, \pm J_y)$ in momentum space instead of traditional two points [56] when $J_x = 0$, if we do not consider the Gaussian profile $\Phi_0$.

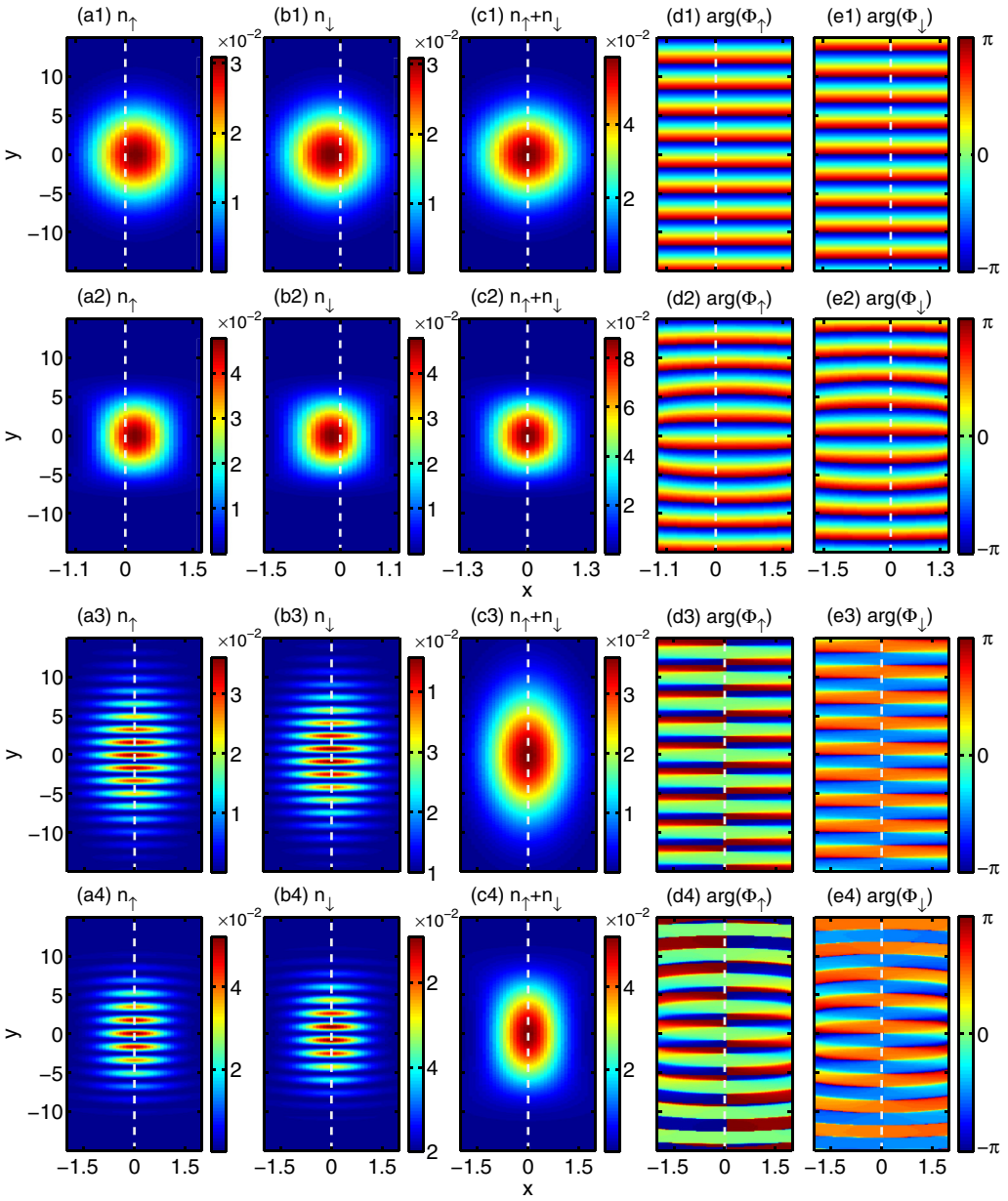


FIG. 1. (Color online) Profiles of the density $n_{\uparrow,\downarrow} = |\Phi_{\uparrow,\downarrow}|^2$ of (a) spin ↑ and (b) spin ↓, (c) the total density $n_\uparrow + n_\downarrow$, the phase of (d) spin ↑ and (e) spin ↓ for (a1)–(e1) and (a2)–(e2) a plane-wave soliton with $\gamma_{12} = 6$ and (a3)–(e3) and (a4)–(e4) a stripe soliton with $\gamma_{12} = 10$. (a1)–(el) and (a3)–(e3) The solitons are obtained by the variational method. (a2)–(e2) and (a4)–(e4) The solitons are calculated by the imaginary-time evolution of the GPE (9). The dashed white line labels the $x = 0$ line. Here $\gamma = 8$, $\gamma_d/\gamma = 0.67$, and $\alpha = 2$.

We calculate the variational parameters of stripe solitons by performing the minimization of the energy $\mathcal{E}$ in Eq. (8) where $\Phi$ is replaced with $\Phi_S$. The density and phase profiles of a typical stripe soliton calculated by this method are displayed in Figs. 1(a3)–1(e3). Evidently, the density of each component exhibits the stripe structure, while the total density does not. The phase of spin ↑ along the $y$ direction varies like a plane wave, but reverses across $x = 0$ due to the presence of $\sin(J_x x)$ in the imaginary part. The phase of spin ↓ exhibits the phase rotationlike vortices around $x = 0$ and $y = n\pi/J_y$ with an integer $n$; around these points, the wave function $\Phi_{S\downarrow}$ is proportional to $(-1)^n[J_x x + i(J_y y - n\pi)]$ and the corresponding density of spin ↓ is extremely low. Moreover, in Figs. 1(a4)–1(e4), we plot the density and phase profiles of the corresponding stripe soliton obtained by the imaginary-time evolution of the GPE; comparing these figures with Figs. 1(a3)–1(e3) shows that the stripe variational ansatz is qualitatively consistent with the Gross-Pitaevskii results.

To study the properties of a soliton with respect to dipole-dipole interactions $\gamma_d$, we evaluate the variational parameters of both the plane-wave and stripe solitons by the variational method and plot them in Fig. 2 as $\gamma_d/\gamma$ varies. Clearly, with increasing $\gamma_d/\gamma$, $a_x$ and $a_y$ increase monotonically because of the enhanced effective attractive interaction, indicating that the size $l_x$ and $l_y$ of the soliton decrease monotonically. We note that as $\gamma_d/\gamma$ increases further, the soliton can collapse so that both $a_x$ and $a_y$ diverge. For the plane-wave soliton, $a_x$ and $a_y$ are slightly larger than the stripe soliton because

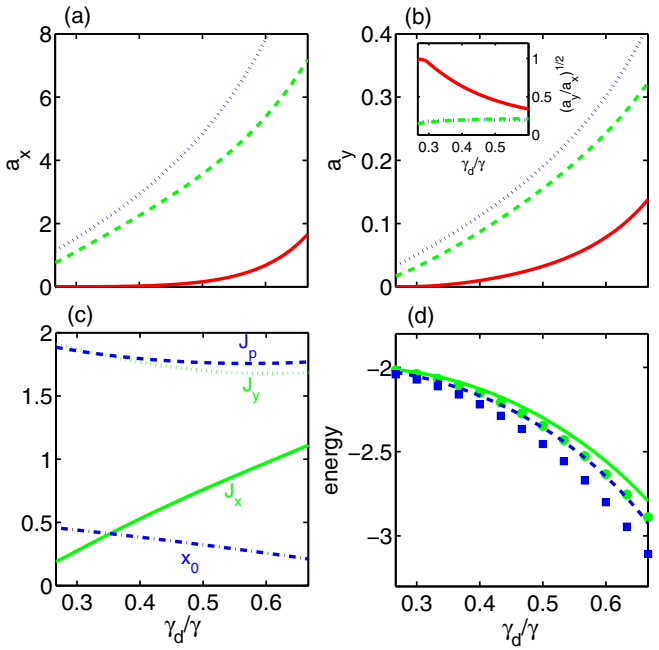


FIG. 2. (Color online) Plot of (a) $a_x$ and (b) $a_y$ as a function of $\gamma_d/\gamma$ for the plane-wave solitons (dotted blue line), stripe solitons (dashed green line), and traditional solitons (solid red line) without spin-orbit coupling. The aspect ratio $\sqrt{a_y/a_x}$ of a soliton is displayed in the inset of (b). (c) Variational parameters with respect $\gamma_d/\gamma$, associated with $x_0$ (dash-dotted blue line) and $J_p$ (dashed blue line) for the plane-wave soliton and $J_x$ (solid green line) and $J_y$ (dotted green line) for the stripe soliton. (d) Total energy of the variational ansatz wave function and the wave function numerically obtained by the imaginary-time evolution of the GPE for both plane-wave and stripe solitons. The solid green line (stripe soliton) and dashed blue line (plane-wave soliton) correspond to the variational results, while the green circles and blue squares correspond to the Gross-Pitaevskii results. Here $\alpha = 2, \gamma = 8$, and $\gamma_{12} = 6\,(\gamma_{12} = 10)$ for the plane-wave (stripe) soliton.

of the smaller contact interaction of the former. Moreover, compared with the soliton without spin-orbit coupling [red line in Figs. 2(a) and 2(b)], $a_x$ and $a_y$ for both the plane-wave and stripe solitons are much larger, implying that the size of solitons can be reduced by spin-orbit coupling. Also, these solitons are highly anisotropic with the much smaller aspect ratio $\sqrt{a_y/a_x}$ as shown in the inset of Fig. 2(b). To elucidate the reason, we explicitly write that single-particle energy of the plane-wave variational ansatz in Eq. (12), which results from the presence of $x_0$ and $J_p$,

$$E_s^{\mathrm{PW}} = \tfrac{1}{2}J_p^2 - \alpha e^{-x_0^2 a_x/4}\left(J_p + \tfrac{1}{2}a_x x_0\right). \tag{17}$$

The minimization of $E_s^{\mathrm{PW}}$ with respect to $x_0$ and $J_p$ for fixed $a_x$ yields

$$x_0 = \frac{-J_p + \sqrt{J_p^2 + 2a_x}}{a_x}, \tag{18}$$

$$J_p = \alpha e^{-x_0^2 a_x/4}. \tag{19}$$

For $a_x = 0$, the energy is independent of $x_0$ and $J_p = \alpha$, while for $a_x \neq 0$, both $x_0$ and $J_p$ decrease slightly with increasing $a_x$

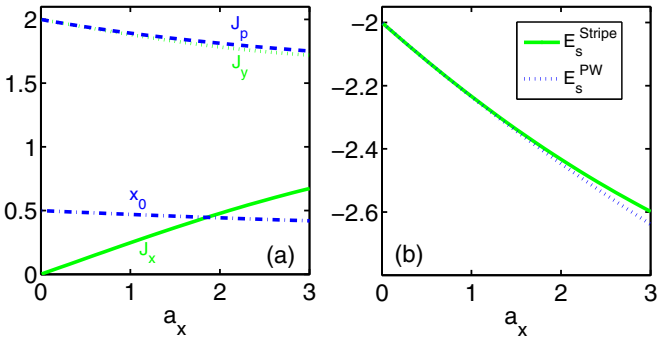


FIG. 3. (Color online) (a) Plot of $x_0$ (dash-dotted blue line) and $J_p$ (dashed blue line) for the plane-wave variational ansatz and $J_x$ (solid green line) and $J_y$ (dotted green line) for the stripe variational ansatz with respect to $a_x$ by the minimization of the energy $E_s^{\mathrm{PW}}$ and $E_s^{\mathrm{stripe}}$. (b) Minimum energy of $E_s^{\mathrm{PW}}$ (dotted blue line) and $E_s^{\mathrm{stripe}}$ (solid green line) as a function of $a_x$. Here $\alpha = 2$.

as shown in Fig. 3(a) with the asymptotic $x_0 = 1/\alpha$ and $J_p = \alpha$ as $a_x$ goes zero. The energy $E_s^{\mathrm{PW}}$ is also a monotonically decreasing function of $a_x$. In addition, this energy decline combined with the reduced dipole-dipole interaction energy competes with the rise of the kinetic energy (when $x_0 = J_p = 0$) and contact interaction energy, leading to an increased $a_x$ and $a_y$ compared with the soliton without spin-orbit coupling. This is also consistent with Fig. 2(c), showing that with increasing dipole-dipole interaction, $a_x$ increases and therefore both $x_0$ and $J_p$ decrease so as to lower $E_s^{\mathrm{PW}}$. It is important to note that although $E_s^{\mathrm{PW}}$ is not a function of $a_y$, other energy such as the kinetic energy (when $x_0 = J_p = 0$), the contact, and dipolar interaction energy depends on it.

For the stripe soliton, the single-particle energy due to the presence of $J_x$ and $J_y$ is

$$E_s^{\mathrm{stripe}} = \tfrac{1}{2}\left(J_x^2 + J_y^2\right) - \alpha\left(J_x + J_y e^{-J_x^2/a_x}\right). \tag{20}$$

Similar to the plane-wave case, this energy is independent of $a_y$. For fixed $a_x$, the minimization of this energy yields both $J_x$ and $J_y$ as a function of $a_x$ as shown in Fig. 3(a). When $a_x$ moves towards zero, the solution approaches $(J_x = \alpha, J_y = 0)$ or $(J_x = 0, J_y = \alpha)$; when it moves away from zero, there is only one solution where $J_y$ decreases from $\alpha$ while $J_x$ increases from zero with the rise of $a_x$. Also, the energy $E_s^{\mathrm{stripe}}$ decreases as $a_x$ increases. Analogous to the plane-wave soliton, the total energy decrease resulting from spin-orbit coupling and dipole-dipole interactions as $a_x$ and $a_y$ increase from the value without spin-orbit coupling exceeds the energy gain of the kinetic (when $J_x = 0$ and $J_y = 0$) and contact interaction; this leads to the increased $a_x$ and $a_y$ compared with the soliton without spin-orbit coupling. This picture is also consistent with Fig. 2(c), where $J_x$ increases while $J_y$ decreases with respect to $\gamma_d/\gamma$.

To explicitly demonstrate the effect of the spin-orbit coupling on the properties of a soliton, we plot the variational parameters as a function of the spin-orbit coupling strength $\alpha$ for both the plane-wave and stripe solitons in Fig. 4. Consistent with the aforementioned feature that spin-orbit coupling can reduce the size of the soliton, both Figs. 4(a) and 4(b) display a monotonic increasing behavior of $a_x$ and $a_y$

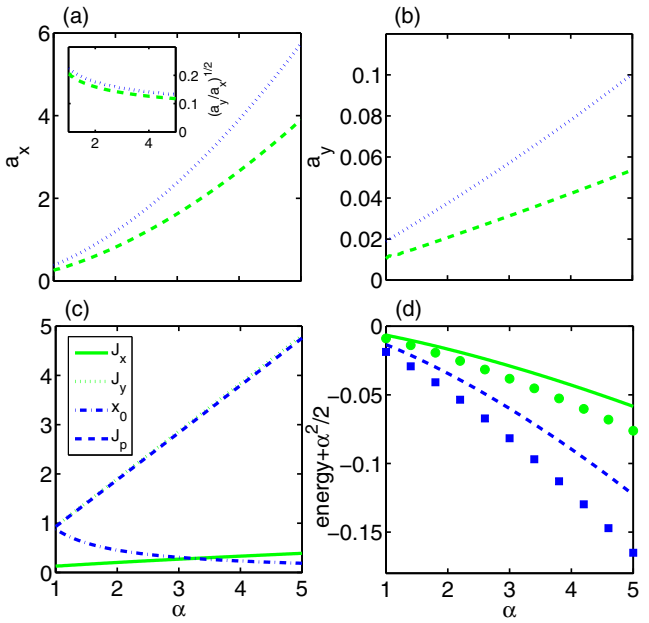


FIG. 4. (Color online) Plot of (a) $a_x$ and (b) $a_y$ as a function of the spin-orbit coupling strength $\alpha$ for the plane-wave soliton (dotted blue line) and stripe soliton (dashed green line). The aspect ratio $\sqrt{a_y/a_x}$ of a soliton is plotted in the inset of (a). (c) Change of $x_0$ (dash-dotted blue line) and $J_p$ (dashed blue line) for the plane-wave soliton and $J_x$ (solid green line) and $J_y$ (dotted green line) for the stripe soliton with respect to $\alpha$. (d) Total energy plus $\alpha^2/2$ plotted as a function of $\alpha$. The solid green (for a stripe soliton) and dashed blue (for a plane-wave soliton) lines are calculated by the variational method, while the green circles (for a stripe soliton) and blue squares (for a plane-wave soliton) are numerically obtained by the imaginary-time evolution of the GPE. Here $\gamma = 8$, $\gamma_d/\gamma = 0.67$, and $\gamma_{12} = 6$ ($\gamma_{12} = 10$) for the plane-wave (stripe) soliton.

as a function of $\alpha$. Also, the aspect ratio $\sqrt{a_y/a_x}$ is decreased by spin-orbit coupling. Similar to Figs. 2(a) and 2(b), $a_x$ and $a_y$ for the plane-wave soliton are slightly larger than the stripe soliton in that the former has a smaller contact interaction. For the plane-wave soliton, $J_P$ (determined mainly by the spin-orbit coupling strength) increases with respect to $\alpha$ while $x_0$ decreases; for the stripe soliton, both $J_x$ and $J_y$ increase.

In Figs. 2(d) and 4(d), for both plane-wave and stripe solitons, we compare their energy obtained by the variational procedure with the one obtained by the imaginary-time evolution of the GPE. Both figures show that the energy calculated by the imaginary-time evolution is lower as expected. Yet the difference between these two energy is not large (no more than 10%), suggesting that the variational ansatz can qualitatively characterize the solitons. We note that in Fig. 4(d), the energy is shifted by $\alpha^2/2$ in order to clearly present the different results of the two methods, which could be smeared by the large value of $\alpha^2/2$.

## IV. MOVING BRIGHT SOLITONS

Generally, the wave function of a moving soliton with the velocity $\mathbf{v}$ can be simply written as $\exp(i\mathbf{v}\cdot\mathbf{r})\Phi_s(\mathbf{r}-\mathbf{v}t)$ (the density does not disperse), where $\Phi_s$ is the wave function of a stationary soliton; however, this is only valid for a system respecting Galilean transform invariance. In fact, Galilean invariance is broken in a spin-orbit-coupled BEC [69] and this violation dictates that the shape of a soliton depends on its velocity strength [56]. Here, for a soliton in a spin-orbit-coupled dipolar BEC in two dimensions, we assume that a moving soliton can be written as

$$\Phi_M(\mathbf{r},t) = \Phi_v(\mathbf{r}',t)\exp\left(i\mathbf{v}\cdot\mathbf{r} - i\tfrac{1}{2}v^2t\right), \tag{21}$$

where $\Phi_v$ is a localized function (the density still does not disperse) and $\mathbf{r}' = \mathbf{r} - \mathbf{v}t$ is the coordinate in the moving frame. Plugging $\Phi_M(\mathbf{r},t)$ into Eq. (9) yields

$$i\frac{\partial\Phi_v(\mathbf{r}',t)}{\partial t} = \mathcal{H}_s(\mathbf{v})\Phi_v(\mathbf{r}',t) + \gamma\mathcal{G}\Phi_v(\mathbf{r}',t) + \frac{\gamma_d}{(2\pi)^2}\int d\mathbf{k}e^{i\mathbf{k}\cdot\mathbf{r}}n(\mathbf{k})U_d(\mathbf{k})\Phi_v(\mathbf{r}',t), \tag{22}$$

where $\mathcal{H}_s(\mathbf{v}) = \mathcal{H}_s + \alpha(\mathbf{v}\times\boldsymbol{\sigma})\cdot\mathbf{e}_z + \mathbf{v}^2/2$. Compared to Eq. (9), this dynamical equation has an additional term $\alpha(\mathbf{v}\times\boldsymbol{\sigma})\cdot\mathbf{e}_z$ (the $\mathbf{v}^2/2$ term has no effects on the dynamics), acting as a Zeeman field; this additional term implies the violation of Galilean invariance. This violation means that it is no longer a trivial task to find a moving bright soliton for a BEC with spin-orbit coupling; we need to perform an imaginary-time evolution of Eq. (22), but not Eq. (9). Furthermore, such a 2D moving soliton should be different for different velocity directions even if their amplitude is the same, in contrast to a 1D soliton, which can only move in one direction.

To examine how the shape of a soliton changes with respect to the velocities along $x$ and $y$ directions, we plot the imbalance $I$ and the width $l_x$ of a soliton of spin $\uparrow$ as a function of the velocities $v_x$ and $v_y$ in Fig. 5. Here the imbalance for spin $\uparrow$ is defined as

$$I = \frac{|\Phi_\uparrow(0)|^2 - |\Phi_\uparrow(\pi/2\alpha)|^2}{|\Phi_\uparrow(0)|^2 + |\Phi_\uparrow(\pi/2\alpha)|^2}, \tag{23}$$

which characterizes a stripe soliton [as shown in Figs. 5(c) and 5(d)] when it approaches one and a plane-wave soliton [as shown in Fig. 5(e) and 5(f)] when it approaches zero. Figures 5(a) and 5(b) demonstrate that $I$ suffers a sharp decline from one to near zero as $v_x$ and $v_y$ increase, indicating that a moving soliton tends to be a plane-wave state. The reason is the broken rotation symmetry of the single-particle Hamiltonian by the velocity induced Zeeman field, giving rise to a ground state of the single-particle system lying at one momentum point located along the $x$ ($y$) direction when the velocity is along that direction. This also explains why the phase of a moving plane-wave soliton with the velocity along the $x$ ($y$) direction varies along that direction.

Furthermore, Fig. 5(a) demonstrates that the width of the soliton gradually grows when the velocity along the $y$ direction is enlarged, To explain the growth, we consider the plane-wave ansatz in Eq. (12), which yields an additional term $-\alpha v_y e^{-a_x x_0^2/4}$ for the single-particle energy when a soliton moves; this energy decrease increases exponentially with the decline of $a_x$ (i.e., increase of the width), leading to an expanded soliton with the rise of the velocity. However, this is not a monotonic behavior and the soliton begins shrinking

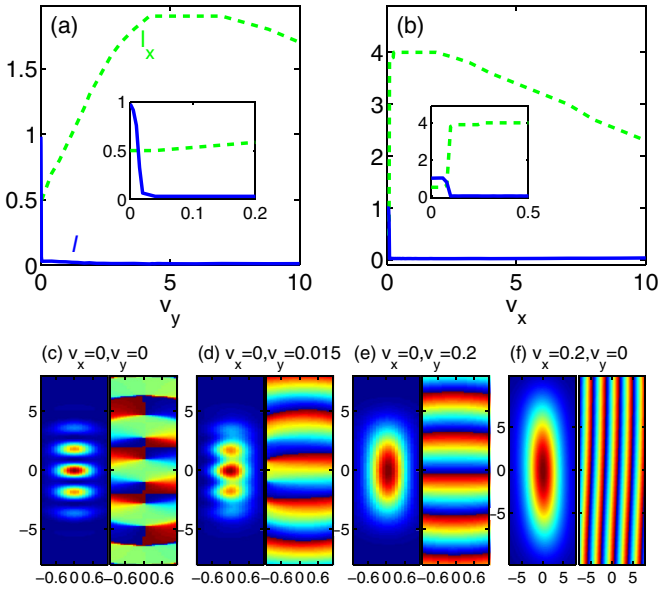


FIG. 5. (Color online) Imbalance $I$ and width $l_x$ of spin $\uparrow$ of the solitons with respect to the velocity along the (a) $y$ and (b) $x$ directions. The insets display the enlarged figure in a small velocity region. Density and phase profiles of four typical moving solitons for spin $\uparrow$ corresponding to the different velocities in (a) and (b) are plotted in (c)–(f) where the horizontal and vertical coordinates are $x'$ and $y'$ respectively. Here $\alpha = 2$, $\gamma = 8$, $\gamma_{12} = 10$, and $\gamma_d/\gamma = 1$, corresponding to a stripe soliton when stationary.

when the velocity becomes larger, due to the enlarged $J_p$ by the velocity-induced Zeeman field, similar to increasing spin-orbit coupling. On the other hand, when the velocity is along the $x$ direction, the width of the soliton increases suddenly as the velocity varies, as shown Fig. 5(b). This corresponds to a change from a stripe soliton with the wave vector along the $y$ direction to a plane-wave soliton with the wave vector along the $x$ direction. For the stationary solitons, the soliton with the wave vector mainly along the $y$ direction has lower energy than the one with the wave vector mainly along the $x$ direction as the dipoles are completely oriented along $y$. However, the Zeeman field induced by the presence of a velocity along the $x$ direction gives rise to the single-particle ground state that possesses the wave vector along $x$. The two states with the wave vector along these two directions compete and change from the former to the latter (i.e., first-order phase transition). For the decrease of the width when $v_x$ becomes even larger, the reason is the same as the case for $v_y$. When a stationary soliton is a plane wave, the moving behavior is similar except that the moving soliton is always the plane-wave soliton.

## V. CONCLUSION

We have studied the bright solitons as the ground states in a spin-orbit-coupled dipolar BEC in two dimensions with dipoles completely polarized along one direction in the 2D plane. It is important to note that the solitons are the ground states in two dimensions, but they are the metastable states in quasi-two-dimensions where the true ground state would collapse and there is an energy barrier between the soliton state and this ground state. Two types of solitons have been found: a plane-wave soliton and a stripe soliton. The former has the plane-wave phase variation and its two components are slightly spatially separated; for the latter, the density of each component is spatially oscillating and the variational ansatz suggests that four points in momentum space are involved. Both plane-wave and stripe solitons are highly anisotropic and their size is decreased by spin-orbit coupling. These solitons cannot exist as the ground states in a 2D system with purely attractive contact interactions and spin-orbit coupling. Moreover, the shape of these solitons changes with their velocities due to the absence of Galilean invariance and this change is anisotropic.

The 2D bright soliton, albeit mainly a plane-wave soliton, can also exist when equal Rashba and Dresselhaus spin-orbit coupling is considered. In experiments, this type of spin-orbit coupling has been engineered by coupling two hyperfine states of atoms through two counterpropagating Raman laser beams [29–34] and such a setup could be employed to realize this spin-orbit coupling in dysprosium [72] with large dipole-dipole interactions. Also, the large magnetic moment in dysprosium atoms may permit the realization of Rashba spin-orbit coupling [80].

## ACKNOWLEDGMENTS

We would like to thank L. Jiang, K. Sun, C. Qu, Z. Zheng, and L. D. Carr for helpful discussions. Y.X. and C.Z. were supported by ARO (Grant No. W911NF-12-1-0334) and AFOSR (Grant No. FA9550-13-1-0045). Y.Z. was supported by Okinawa Institute of Science and Technology Graduate University. We also thank Texas Advanced Computing Center as part of our numerical calculations were performed there.

[1] M. H. Anderson, J. R. Ensher, M. R. Matthews, C. E. Wieman, and E. A. Cornell, Science **269**, 198 (1995).

[2] K. B. Davis, M.-O. Mewes, M. R. Andrews, N. J. van Druten, D. S. Durfee, D. M. Kurn, and W. Ketterle, Phys. Rev. Lett. **75**, 3969 (1995).

[3] C. J. Pethick and H. Smith, *Bose-Einstein Condensation in Dilute Gases*, 2nd ed. (Cambridge University Press, Cambridge, 2008).

[4] P. G. Kevrekidis, D. J. Frantzeskakis, and R. Carretero-González, *Emergent Nonlinear Phenomena in Bose-Einstein Condensates* (Springer, Berlin, 2007).

[5] C. Chin, R. Grimm, P. Julienne, and E. Tiesinga, Rev. Mod. Phys. **82**, 1225 (2010).

[6] S. Burger, K. Bongs, S. Dettmer, W. Ertmer, K. Sengstock, A. Sanpera, G. V. Shlyapnikov, and M. Lewenstein, Phys. Rev. Lett. **83**, 5198 (1999).

[7] J. Denschlag, J. E. Simsarian, D. L. Feder, C. W. Clark, L. A. Collins, J. Cubizolles, L. Deng, E. W. Hagley, K. Helmerson, W. P. Reinhardt, S. L. Rolston, B. I. Schneider, and W. D. Phillips, Science **287**, 97 (2000).

[8] B. P. Anderson, P. C. Haljan, C. A. Regal, D. L. Feder, L. A. Collins, C. W. Clark, and E. A. Cornell, Phys. Rev. Lett. **86**, 2926 (2001).

[9] K. E. Strecker, G. B. Partridge, A. G. Truscott, and R. G. Hulet, Nature (London) **417**, 150 (2002).

[10] L. Khaykovich, F. Schreck, G. Ferrari, T. Bourdel, J. Cubizolles, L. D. Carr, Y. Castin, and C. Salomon, Science **296**, 1290 (2002).

[11] S. L. Cornish, S. T. Thompson, and C. E. Wieman, Phys. Rev. Lett. **96**, 170401 (2006).

[12] B. Eiermann, T. Anker, M. Albiez, M. Taglieber, P. Treutlein, K.-P. Marzlin, and M. K. Oberthaler, Phys. Rev. Lett. **92**, 230401 (2004).

[13] C. Hamner, Y. Zhang, J. J. Chang, C. Zhang, and P. Engels, Phys. Rev. Lett. **111**, 264101 (2013).

[14] J. H. V. Nguyen, P. Dyke, D. Luo, B. A. Malomed, and R. G. Hulet, Nat. Phys. **10**, 918 (2014).

[15] The energy of a 2D system with contact interactions is $(\frac{\hbar^2}{4m} - \frac{g}{2\pi})/L^2$, where the first and second terms are, respectively, the kinetic energy and contact attractive interaction (i.e., $g > 0$) energy, if the ground state is assumed to be $e^{-(x^2+y^2)/2L^2}/\sqrt{\pi}L$ with the size $L$ of the state. When $g < \hbar^2\pi/2m$, the ground state corresponds to $L \to \infty$ (expansion instability); when $g > \hbar^2\pi/2m$, $L \to 0$ (collapse instability). See also Ref. [4].

[16] W. Krolikowski, O. Bang, J. J. Rasmussen, and J. Wyller, Phys. Rev. E **64**, 016612 (2001).

[17] T. Lahaye, C. Menotti, L. Santos, M. Lewenstein, and T. Pfau, Rep. Prog. Phys. **72**, 126401 (2009).

[18] P. Pedri and L. Santos, Phys. Rev. Lett. **95**, 200404 (2005).

[19] I. Tikhonenkov, B. A. Malomed, and A. Vardi, Phys. Rev. Lett. **100**, 090406 (2008).

[20] C. Ticknor, R. M. Wilson, and J. L. Bohn, Phys. Rev. Lett. **106**, 065301 (2011).

[21] M. A. Baranov, M. Dalmonte, G. Pupillo, and P. Zoller, Chem. Rev. **112**, 5012 (2012).

[22] A. Griesmaier, J. Werner, S. Hensler, J. Stuhler, and T. Pfau, Phys. Rev. Lett. **94**, 160401 (2005).

[23] T. Koch, T. Lahaye, J. Metz, B. Frhlich, A. Griesmaier, and T. Pfau, Nat. Phys. **4**, 218 (2008).

[24] Q. Beaufils, R. Chicireanu, T. Zanon, B. Laburthe-Tolra, E. Maréchal, L. Vernac, J.-C. Keller, and O. Gorceix, Phys. Rev. A **77**, 061601(R) (2008).

[25] M. Lu, N. Q. Burdick, S. H. Youn, and B. L. Lev, Phys. Rev. Lett. **107**, 190401 (2011).

[26] K. Aikawa, A. Frisch, M. Mark, S. Baier, A. Rietzler, R. Grimm, and F. Ferlaino, Phys. Rev. Lett. **108**, 210401 (2012).

[27] M. Lu, N. Q. Burdick, and B. L. Lev, Phys. Rev. Lett. **108**, 215301 (2012).

[28] K. Aikawa, A. Frisch, M. Mark, S. Baier, R. Grimm, and F. Ferlaino, Phys. Rev. Lett. **112**, 010404 (2014).

[29] Y.-J. Lin, K. Jiménez-García, and I. B. Spielman, Nature (London) **471**, 83 (2011).

[30] P. Wang, Z.-Q. Yu, Z. Fu, J. Miao, L. Huang, S. Chai, H. Zhai, and J. Zhang, Phys. Rev. Lett. **109**, 095301 (2012).

[31] L. W. Cheuk, A. T. Sommer, Z. Hadzibabic, T. Yefsah, W. S. Bakr, and M. W. Zwierlein, Phys. Rev. Lett. **109**, 095302 (2012).

[32] J.-Y. Zhang, S.-C. Ji, Z. Chen, L. Zhang, Z.-D. Du, B. Yan, G.-S. Pan, B. Zhao, Y.-J. Deng, H. Zhai, S. Chen, and J.-W. Pan, Phys. Rev. Lett. **109**, 115301 (2012).

[33] C. Qu, C. Hamner, M. Gong, C. Zhang, and P. Engels, Phys. Rev. A **88**, 021604(R) (2013).

[34] R. A. Williams, M. C. Beeler, L. J. LeBlanc, K. Jiménez-García, and I. B. Spielman, Phys. Rev. Lett. **111**, 095301 (2013).

[35] T. D. Stanescu, B. Anderson, and V. Galitski, Phys. Rev. A **78**, 023616 (2008).

[36] C. Wang, C. Gao, C.-M. Jian, and H. Zhai, Phys. Rev. Lett. **105**, 160403 (2010).

[37] C. Wu, I. Mondragon-Shem, and X. F. Zhou, Chinese Phys. Lett. **28**, 097102 (2011).

[38] T.-L. Ho and S. Zhang, Phys. Rev. Lett. **107**, 150403 (2011).

[39] S. Sinha, R. Nath, and L. Santos, Phys. Rev. Lett. **107**, 270401 (2011).

[40] Y. Zhang, L. Mao, and C. Zhang, Phys. Rev. Lett. **108**, 035302 (2012).

[41] H. Hu, B. Ramachandhran, H. Pu, and X. J. Liu, Phys. Rev. Lett. **108**, 010402 (2012).

[42] Y. Li, L. P. Pitaevskii, and S. Stringari, Phys. Rev. Lett. **108**, 225301 (2012).

[43] Z. Chen and H. Zhai, Phys. Rev. A **86**, 041604(R) (2012).

[44] K. Sun, C. Qu, and C. Zhang, Phys. Rev. A **91**, 063627 (2015).

[45] C. Qu, K. Sun, and C. Zhang, Phys. Rev. A **91**, 053630 (2015).

[46] Y. Xu, F. Zhang, and C. Zhang, arXiv:1411.7316.

[47] J. Dalibard, F. Gerbier, G. Juzeliunas, and P. Öhberg, Rev. Mod. Phys. **83**, 1523 (2011).

[48] V. Galitski and I. B. Spielman, Nature (London) **494**, 49 (2013).

[49] X. Zhou, Y. Li, Z. Cai, and C. Wu, J. Phys. B **46**, 134001 (2013).

[50] N. Goldman, G. Juzeliūnas, P. Öhberg, and I. B. Spielman, Rep. Prog. Phys. **77**, 126401 (2014).

[51] H. Zhai, Rep. Prog. Phys. **78**, 026001 (2015).

[52] W. Yi, W. Zhang, and X. Cui, Sci. China Phys. Mech. Astron. **58**, 1 (2014).

[53] J. Zhang, H. Hu, X.-J. Liu, and H. Pu, Annu. Rev. Cold At. Mol. **2**, 81 (2014).

[54] Y. Xu and C. Zhang, Int. J. Mod. Phys. B **29**, 1530001 (2015).

[55] M. Merkl, A. Jacob, F. E. Zimmer, P. Öhberg, and L. Santos, Phys. Rev. Lett. **104**, 073603 (2010).

[56] Y. Xu, Y. Zhang, and B. Wu, Phys. Rev. A **87**, 013614 (2013).

[57] V. Achilleos, D. J. Frantzeskakis, P. G. Kevrekidis, and D. E. Pelinovsky, Phys. Rev. Lett. **110**, 264101 (2013).

[58] L. Salasnich and B. A. Malomed, Phys. Rev. A **87**, 063625 (2013).

[59] H. Sakaguchi and B. A. Malomed, Phys. Rev. E **90**, 062922 (2014).

[60] L. Salasnich, W. B. Cardoso, and B. A. Malomed, Phys. Rev. A **90**, 033629 (2014).

[61] H. Sakaguchi, B. Li, and B. A. Malomed, Phys. Rev. E **89**, 032920 (2014).

[62] O. Fialko, J. Brand, and U. Zülicke, Phys. Rev. A **85**, 051605(R) (2012).

[63] V. Achilleos, J. Stockhofe, P. G. Kevrekidis, D. J. Frantzeskakis, and P. Schmelcher, Europhys. Lett. **103**, 20002 (2013).

[64] Y. V. Kartashov, V. V. Konotop, and F. K. Abdullaev, Phys. Rev. Lett. **111**, 060402 (2013).

[65] V. E. Lobanov, Y. V. Kartashov, and V. V. Konotop, Phys. Rev. Lett. **112**, 180403 (2014).
[66] Y. Zhang, Y. Xu, and T. Busch, Phys. Rev. A **91**, 043629 (2015).
[67] Y. Xu, L. Mao, B. Wu, and C. Zhang, Phys. Rev. Lett. **113**, 130404 (2014).
[68] X.-J. Liu, Phys. Rev. A **91**, 023610 (2015).
[69] Q. Zhu, C. Zhang, and B. Wu, Europhys. Lett. **100**, 50003 (2012).
[70] Q. Zhu and B. Wu, Chinese Phys. B **24**, 050507 (2015).
[71] Y. Deng, J. Cheng, H. Jing, C.-P. Sun, and S. Yi, Phys. Rev. Lett. **108**, 125301 (2012).
[72] X. Cui, B. Lian, T.-L. Ho, B. L. Lev, and H. Zhai, Phys. Rev. A **88**, 011601(R) (2013).
[73] H. T. Ng, Phys. Rev. A **90**, 053625 (2014).
[74] Y. Yousefi, E. Ö. Karabulut, F. Malet, J. Cremon, and S. M. Reimann, Eur. Phys. J. Special Topics **224**, 545 (2015).
[75] S. Gopalakrishnan, I. Martin, and E. A. Demler, Phys. Rev. Lett. **111**, 185304 (2013).
[76] R. M. Wilson, B. M. Anderson, and C. W. Clark, Phys. Rev. Lett. **111**, 185303 (2013).
[77] S.-W. Song, Y.-C. Zhang, L. Wen, and H. Wang, J. Phys. B **46**, 145304 (2013).
[78] This elongated configuration along with the wave vector in the $y$ direction has the lower single-particle energy contributed by the spin-orbit coupling than the case with the wave vector in the $x$ direction.
[79] This energy is generally so small that the states with different $\varphi$ are nearly degenerate. That might be the reason why the stripe state for $\varphi = 0$ that possesses a sharp phase change across the symmetric axis in a harmonically trapped spin-orbit-coupled BEC has not been noticed [40].
[80] D. L. Campbell, G. Juzeliūnas, and I. B. Spielman, Phys. Rev. A **84**, 025602 (2011).